Korean J. Chem. Eng., 34(7), 2065-2071 (2017)
DOI: 10.1007/s11814-017-0092-3

pISSN: 0256-1115
eISSN: 1975-7220

Mechanism of Ce promoting SO_2 resistance of MnO_x/γ-Al_2O_3: An experimental and DFT study

Xiaopeng Zhang*, Zhuofeng Li*, Jijun Zhao, Yuezong Cui*, Bojian Tan*, Jinxin Wang*, Chengxiang Zhang*, and Gaohong He*,†**

*School of Petroleum and Chemical Engineering, State Key Laboratory of Fine Chemicals, Dalian University of Technology, Panjin 124221, Liaoning, China
**Key Laboratory of Materials Modification by Laser, Ion and Electron Beams (Dalian University of Technology), Ministry of Education, Dalian 116024, China
(*Received 6 July 2016 • accepted 1 April 2017*)

Abstract−Various physico-chemical techniques and theoretical chemistry computations are used to obtain a deep insight into the mechanism of Ce improving SO_2 resistance of the catalyst $Mn_{0.4}Ce_x/Al_2O_3$ (x stands for the molar ratio of Ce : Al). Theoretical computation with density functional theory (DFT) shows that Ce modification enhances the adsorption energy of SO_2 adsorbed on Ce surrounding, resulting in the preferential adsorption of SO_2 on Ce surrounding. It protects the surface Mn from SO_2 poisoning, leading to a better SO_2 resistance. FT-IR and TG results are in good accordance with DFT results. FT-IR results suggest that absorption peaks related to SO_4^{2-} cannot be detected in $Mn_{0.4}Ce_{0.12}/Al_2O_3$. Moreover, TG results show that weight loss peaks due to sulfated MnO_x decomposition disappears after Ce addition. Therefore, Ce modification inhibits sulfates formation on active components lead to a better resistance to SO_2 of $Mn_{0.4}Ce_{0.12}/Al_2O_3$.

Keywords: Selective Catalytic Reduction, MnO_x, Density Functional Theory, Modification, SO_2 Poisoning

INTRODUCTION

Selective catalytic reduction (SCR) with NH_3 in the presence of oxygen is a feasible technique to reduce NO_x emissions in stationary power plants [1]. V_2O_5-WO_3/TiO_2 catalysts are most commonly adopted [2,3]. To avoid reheat flue gas, the SCR unit has to be located upstream of the desulfurizer and the electrostatic precipitator resulting in a deactivation of catalysts due to dust and alkali metals in flue gas. Low-temperature SCR catalysts can be located downstream and help to prevent the SCR unit from suffering these problems.

MnO_x based catalysts supported on various supports such as TiO_2 [1,2], TiO_2-pillared clay [4], γ-Al_2O_3 [5-7], (active carbon) AC [8], Ce-ZrO_2 [9,10] and some other non-supported catalysts, Mn-Ce [11,12], MnO_2-Fe_2O_3-CeO_2-TiO_2 [13] have been reported in recent years, and these MnO_x based catalysts were found to have an excellent SCR activity at low temperature. Unfortunately, there are still a few amounts of SO_2 even after the desulfurizer. MnO_x based catalysts are sensitive to SO_2 and can be deactivated by formation of sulfite and sulfate species on the catalyst surface [14].

Modifying with cerium can improve SO_2 resistance for MnO_x based catalysts to a certain extent. Cao et al. [15] prepared Fe-Mn-Ce/γ-Al_2O_3 using the sol-gel method and found that the catalyst had a favorable SO_2 and H_2O resistance and the SCR activity remained above 75% in the presence of SO_2 and H_2O. Some other MnO_x based catalysts doped with cerium such as Mn-Ce/γ-Al_2O_3 [7], MnO_x/CeO_2-TiO_2 [2], MnO_2-Fe_2O_3-CeO_2-TiO_2 [13], Mn/Ce-ZrO_2 [16] also show a better SO_2 resistance. The mechanism of cerium improving SO_2 resistance has been researched. Chang et al. [11] investigated the resistance to SO_2 of MnO_x-CeO_2 and pointed out that the high concentration of surface oxygen vacancy corresponded to a better SO_2 resistance. Zhang et al. [17] prepared CeO_2 catalysts modified with solid acid and found that the resistance to H_2O and SO_2 of the catalysts depended on the improvement of surface acidity. Wu et al. [18] and Jin et al. [19] pointed out that cerium addition improved the dissociation of ammonium sulfate on the catalyst surface, resulting in a better SO_2 resistance. SO_2 poisoning starts with the adsorption of SO_2 on the catalyst surface, and then reacts with NH_3 or catalyst components to form some sulfite or sulfate species. This process is closely related to the surface structure of catalysts. Ce doping changes the surface structural properties of catalysts [2,20], which may affect the SO_2 adsorption and the stability of sulfite or sulfate species on the catalyst surface and then affect the SO_2 resistance. However, very little information about this part was available in previous studies.

Therefore, in this work, MnO_x/γ-Al_2O_3 catalyst doped with CeO_2 was prepared and used to remove NO at low temperature in the presence of SO_2. DFT calculation and physicochemical characterizations were performed to get a deep insight into the Ce doping effect on SO_2 adsorption and the stability of sulfite or sulfate species on catalysts surface and to reveal the mechanism of Ce improving SO_2 resistance of the catalyst.

1. Experimental

1-1. Preparation of Supports and Catalysts

Catalyst support was prepared by precipitation method. $Al(NO_3)_3$,

†To whom correspondence should be addressed.
E-mail: hgaohong@dlut.edu.cn

$9H_2O$ as a precursor was dissolved in distilled water. An aqueous solution of ammonia with 25 wt% as the precipitator was added dropwise into the solution until the pH was up to 10. The resulting precipitate was stirred for 3 h and then aged for 1 h and finally filtered, washed, and dried in water bath at 80 °C overnight to get support powder.

Catalysts were prepared by impregnating support powder with $Mn(NO_3)_2$ solution or mixed solutions of $Mn(NO_3)_2$ and $Ce(NO_3)_3 \cdot 6H_2O$ for 12 h. Then the samples were dried in water bath at 80 °C overnight and dried in drying oven at 110 °C for 6 h and finally were calcined in muffle at 500 °C for 6 h. The catalysts were denoted as Mn_xCe_y/Al_2O_3, where x and y stand for the molar ratios of Mn : Al and Ce : Al.

All chemicals were obtained from Tianjin Guangfu Fine Chemical Research Institute (China).

1-2. Characterization of Supports and Catalysts

BET surface areas of the catalysts were measured by nitrogen adsorption at −196 °C using a Autosorb-iQ-C automated gas sorption system (Quantachrome Instruments, USA). The pore size distribution was calculated from the desorption branch of the N_2 adsorption isotherm using the Barrett-Joyner-Halenda (BJH) formula. Prior to the measurements, all samples were outgassed at 300 °C for 2 h.

The powder X-ray diffraction (XRD) measurement was used to identify the crystal structure of the catalysts with XRD-7000 S system using Cu $K\alpha$ radiation (40 kV, 100 mA) (SHIMADZU Corporation, Japan). Diffraction patterns were obtained over a 2θ range of 8-80°, at a scan speed of 5° min^{-1} and a step of 0.02°.

The change of the relative atomic concentration on the surface of the catalysts were obtained by the X-ray photoelectron spectroscopy using a ESCALAB250 (Thermo Fisher Scientific Corporation, USA) with monochromatic AlKa radiation. Sample charging effects were eliminated by correcting the observed spectra with the C 1s binding energy value of 284.6 eV.

FT-IR spectra were acquired with a Nicolet iN10 MX & iS10 (ThermoFisher) FT-IR spectrometer using a thin self-supporting sample wafer accumulation of 100 scans running at 4 cm^{-1} resolution.

Thermogravimetric analyses (TGA) were performed on 0.01 g of sample with a NETZSCH thermal analysis system under a nitrogen flow of 20 mL/min, using a heating rate of 10 °C/min from room temperature to 900 °C (NETZSCH Corporation, Germany).

1-3. Catalytic Activity Test

The SCR activity measurement was performed in a fixed-bed flow reactor (Fig. S1). The concentrations of simulated gases were as follow: 600 ppm NO, 600 ppm NH_3, 3 vol% O_2, 3 vol% H_2O (when used), 100 ppm SO_2 (when used) and N_2 as balance gas. In all the runs, the total gas flow rate was 300 mL/min and the gas hourly space velocity (GHSV) was about 45,000 h^{-1}. The feed gases were mixed and preheated in a chamber before entering the reactor. The water vapor was generated by passing N_2 through a gas-wash bottle containing deionized water. During the measurements, the concentrations of NO at the inlet and outlet of the reactor were monitored by flue gas analyzer (KM950, Kane International Ltd., United Kingdom). The concentration of N_2O was measured by FTIR (WQF-510A, Beijing Rayleigh Analytical Instrument Co., Ltd.) equipped with a gas sample cell. The NO conversion was calculated using the following equation:

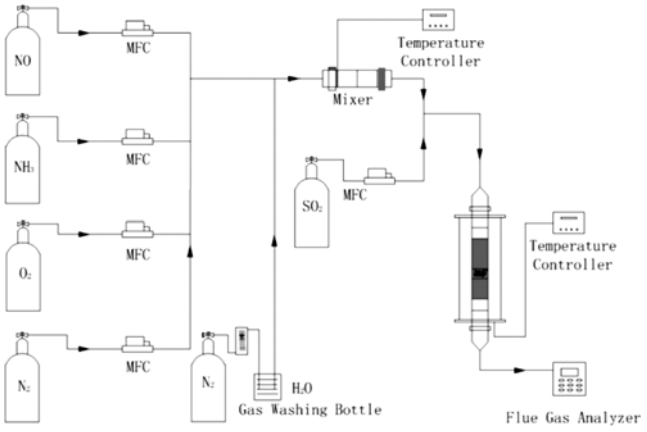

Fig. 1. Schematic diagram of the experimental setup.

$$\text{NO conversion } \% = \frac{NO_{in} - NO_{out}}{NO_{in}} \times 100\%$$

NO_{in}: inlet NO_x concentration (ppm); NO_{out}: outlet NO_x concentration (ppm)

1-4. Models and Computational Details

All calculations were carried out with the Material Studio modelling Dmol3 package [21,22]. Double numerical plus polarization function (the DNP basis set) and the generalized gradient approximation (GGA) with PBE functional were used in all calculations [22,23]. And the real space cut-off radius was maintained as 5.8 Å. The core electrons were treated with DFT semi-core pseudopotentials. Models were built with six atomic layers with two bottom layers fixed and four top layers relaxed. The vacuum region was set to be 18 Å. The lattice constant of MnO_2 is a=b=4.3983, c=2.8730 Å and $\alpha=\beta=\gamma=90°$ [24]. And that of CeO_2 is a=b=c=5.411 Å and $\alpha=\beta=\gamma=90°$ [25]. The tolerance of energy is 0.00027 eV, gradient is 0.054 eV/Å, smearing is 0.136 eV, and displacement convergence is 0.005 Å.

The adsorption energy (Eads) was calculated as follows: $E_{ads}=E_{SO_2/Surface}-(E_{SO_2}+E_{Surface})$, where $E_{Surface}$ is the total energy of bare MnO_2 (110) or CeO_2 (110), E_{SO_2} is the energy of an isolated SO_2 molecule and $E_{SO_2/Surface}$ is the total energy of the same molecule adsorbed on surface.

RESULTS AND DISCUSSION

1. Catalytic Activity Results

NO conversions of the catalysts in temperature range from 80 to 240 °C are shown in Fig. 2(a). The activity for $Mn_{0.4}/\gamma\text{-}Al_2O_3$ increased with the increase of temperature, reached a maximum value 99.5% at 180 °C and then decreased. After the addition of Ce, the SCR activity was dramatically improved, especially at low temperature. NO removal efficiency of $Mn_{0.4}Ce_{0.12}/\gamma\text{-}Al_2O_3$ was 70.8% at 80 °C, which was 41.7% more than that of $Mn_{0.4}/\gamma\text{-}Al_2O_3$ at the same temperature. And it maintained at 100% in the temperature range of 100-240 °C.

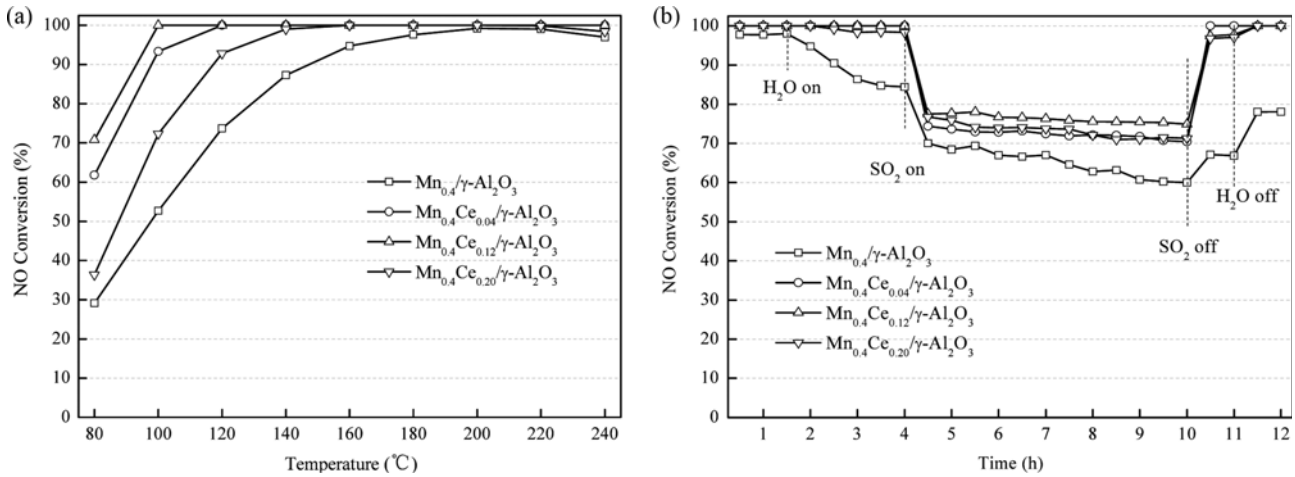

Fig. 2. (a) SCR activity of different catalysts (b) Effect of H_2O and SO_2 on SCR activity of different catalysts at 180 °C of different catalysts.

There was still a small amount of SO_2 and H_2O in flue gases after desulfurization, which may inhibit SCR activity to some degree. Therefore, an experiment was designed to investigate the effect of SO_2 and H_2O on the SCR activity, and the results are illustrated in Fig. 2(b). For $Mn_{0.4}/\gamma$-Al_2O_3, the activity decreased slowly from 98.0% to 84.4% in 2.5 h after the addition of H_2O. When SO_2 was added into the flue gas, the activity sharply decreased from 84.4% to 70.0% in the first 0.5 h and then the activity declined slowly to 60% during 5.5 h. When SO_2 and H_2O were cut off, the activity partly recovered. After Ce doping, the NO removal efficiency for these catalysts remained at about 100% in the presence of H_2O at 180 °C. When SO_2 was injected, the activity decreased to 70.0% in the first 0.5 h and then kept stable. When SO_2 and H_2O were cut off, the activity totally recovered to the original level. Compared to $Mn_{0.4}Ce_{0.04}/\gamma$-Al_2O_3 and $Mn_{0.4}Ce_{0.2}/\gamma$-Al_2O_3, $Mn_{0.4}Ce_{0.12}/\gamma$-Al_2O_3 had a little higher NO removal efficiency in the presence of SO_2 and H_2O. These results suggested that Ce doping, especially when the ratio Ce : Al was 0.12 : 1, significantly improved the resistance to H_2O and SO_2 of the catalyst.

2. Catalyst Characterization and DFT Calculation

2-1. BET and XRD Analysis

The BET surface area, pore volume, and pore size of different samples are summarized in Table 1. The BET surface area pore volume, and pore size of $Mn_{0.4}/\gamma$-Al_2O_3 was 175.4 m^2/g, 0.269 cm^3/g and 6.13 nm, respectively. Ce addition could enhance BET surface area and pore size and the maximum values turned up in $Mn_{0.4}Ce_{0.12}/\gamma$-Al_2O_3 which were 231.8 m^2/g and 0.380 cm^3/g, respectively. It indicated that, to certain extent, Ce addition could improve the dispersion of MnO_2. However, when Ce loading amount further increased, BET surface area and pore size decreased. Pure ceria has been known to be poorly thermostable and easily sintering under high temperature [26,27]. Excessive Ce loading might wenken the interaction between Ce and Mn, resulting in Ce sintering and a small BET surface area and pore size.

Table 1. Specific surface area and pore structure of the catalyst

Sample	BET surface area (m^2/g)	Pore volume (cm^3/g)	Pore size (nm)
$Mn_{0.4}/\gamma$-Al_2O_3	175.4	0.269	6.13
$Mn_{0.4}Ce_{0.04}/\gamma$-Al_2O_3	200.0	0.364	7.28
$Mn_{0.4}Ce_{0.12}/\gamma$-Al_2O_3	231.8	0.380	6.56
$Mn_{0.4}Ce_{0.20}/\gamma$-Al_2O_3	175.1	0.289	6.59

XRD patterns of the catalysts are shown in Fig. 3. Four sharp and strong peaks at 2θ=28.7, 37.1, 42.4, 56.6, 66.0, 72.3 were detected in the catalyst $Mn_{0.4}/\gamma$-Al_2O_3 and were attributed to the phase of MnO_2 (JCPDS no. 30-0820 and 24-0735). After Ce addition, those peaks became much weaker due to the interaction between Ce and Mn [18,28]. When Ce loading amount reached 0.2, MnO_2 diffraction peaks became strong. These results suggest that the optimal Ce loading amount for $Mn_{0.4}/\gamma$-Al_2O_3 was 0.12. The grain size of MnO_2 in $Mn_{0.4}/\gamma$-Al_2O_3, $Mn_{0.4}Ce_{0.04}/\gamma$-Al_2O_3, $Mn_{0.4}Ce_{0.12}/\gamma$-Al_2O_3 and $Mn_{0.4}Ce_{0.2}/\gamma$-Al_2O_3 was 92.4, 79.8, 67.4 and 84.0 Å, respectively, which were calculated by the Scherrer Formula and K value was 0.943. Note that values of grain size obtained from the Scher-

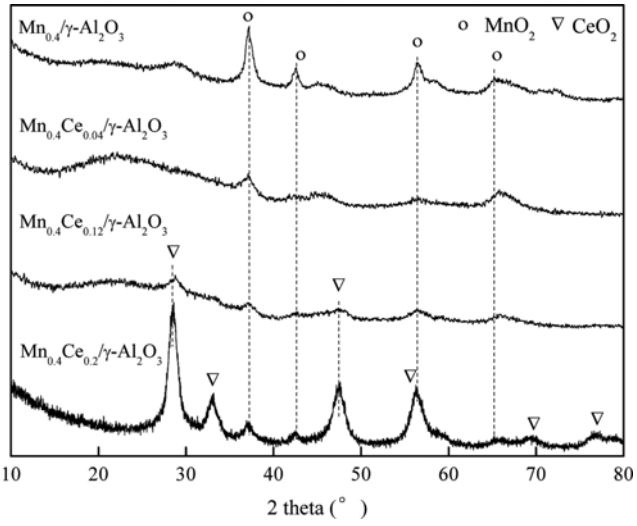

Fig. 3. XRD patterns of different catalysts.

rer formula were not accurate, but from these results we could still tell the better dispersion of MnO_2 in $Mn_{0.4}Ce_{0.12}/\gamma$-Al_2O_3 because of Ce adding. Compared to $Mn_{0.4}/\gamma$-Al_2O_3, new peaks at 2θ=28.5, 33.1, 47.5, 56.3, 69.4 and 76.7 were detected in the catalyst $Mn_{0.4}Ce_{0.2}/\gamma$-Al_2O_3 and were attributed to the phase of CeO_2 (JCPDS no. 43-1002). But for $Mn_{0.4}Ce_{0.04}/\gamma$-Al_2O_3 and $Mn_{0.4}Ce_{0.12}/\gamma$-Al_2O_3, CeO_2 diffraction peaks were not apparent and even could not be detected. Those results indicated that Ce modification could improve the dispersion of MnO_2, but when the Ce loading amount increased, both CeO_2 and MnO_2 dispersion got worse. The high dispersion and poor crystal structure CeO_2 and MnO_2 in $Mn_{0.4}Ce_{0.12}/\gamma$-Al_2O_3 were favorable for the SCR activity as reported in previous works [29,30].

2-2. XPS Analysis

XPS analyses were performed to identify the surface properties of the catalysts. The XPS spectra of Mn 2p, Ce 3d and O 1s are shown in Fig. 4 and the surface atomic concentrations are shown in Table 2.

Two peaks due to Mn $2p_{1/2}$ and Mn $2p_{3/2}$ were observed in Mn 2p spectra. The Mn $2p_{3/2}$ spectra could be separated into two fitting peaks around 640.5 eV and 642.2 eV, which could be assigned to Mn_2O_3 and MnO_2, respectively [31]. It indicated that Mn^{3+} and Mn^{4+} co-existed on the catalyst surface. Ce 3d spectra were complicated. The peaks denoted by u′, v′ were assigned to Ce^{3+} and the other peaks denoted by u, u″, u‴, v, v″, v‴ were assigned to Ce^{4+} [32,33]. From these peaks, CeO_2 was the major phase and the peaks corresponding to Ce^{4+} became stronger with the increase of Ce loading. Only one main peak was detected in O 1s spectra, which could be deconvoluted into two sub-bands. The peaks at 529.3-529.9 eV and 531.3-531.7 eV were corresponding to lattice oxygen (denoted as O″) and surface adsorbed oxygen (denoted as O′), respectively [34]. As shown in Table 2, the surface concentrations of O′ and Mn^{4+} increased after Ce addition, and the maximum values turned up in $Mn_{0.4}Ce_{0.12}/\gamma$-Al_2O_3.

Table 2. The surface atomic concentration of the catalysts

Sample	O (%)		Ce (%)		Mn (%)	
	O′	O″	Ce^{3+}	Ce^{4+}	Mn^{3+}	Mn^{4+}
$Mn_{0.4}/\gamma$-Al_2O_3	22.86	19.38	-	-	1.87	1.87
$Mn_{0.4}Ce_{0.04}/\gamma$-Al_2O_3	23.49	17.65	0.20	0.60	1.56	2.15
$Mn_{0.4}Ce_{0.12}/\gamma$-Al_2O_3	24.11	16.07	0.30	1.15	1.44	2.24
$Mn_{0.4}Ce_{0.2}/\gamma$-Al_2O_3	22.49	17.28	0.51	2.47	1.08	1.00

The main reason for the inhibition of SO_2 for SCR activity at low temperature is that SO_2 can react with NH_3 forming ammo-

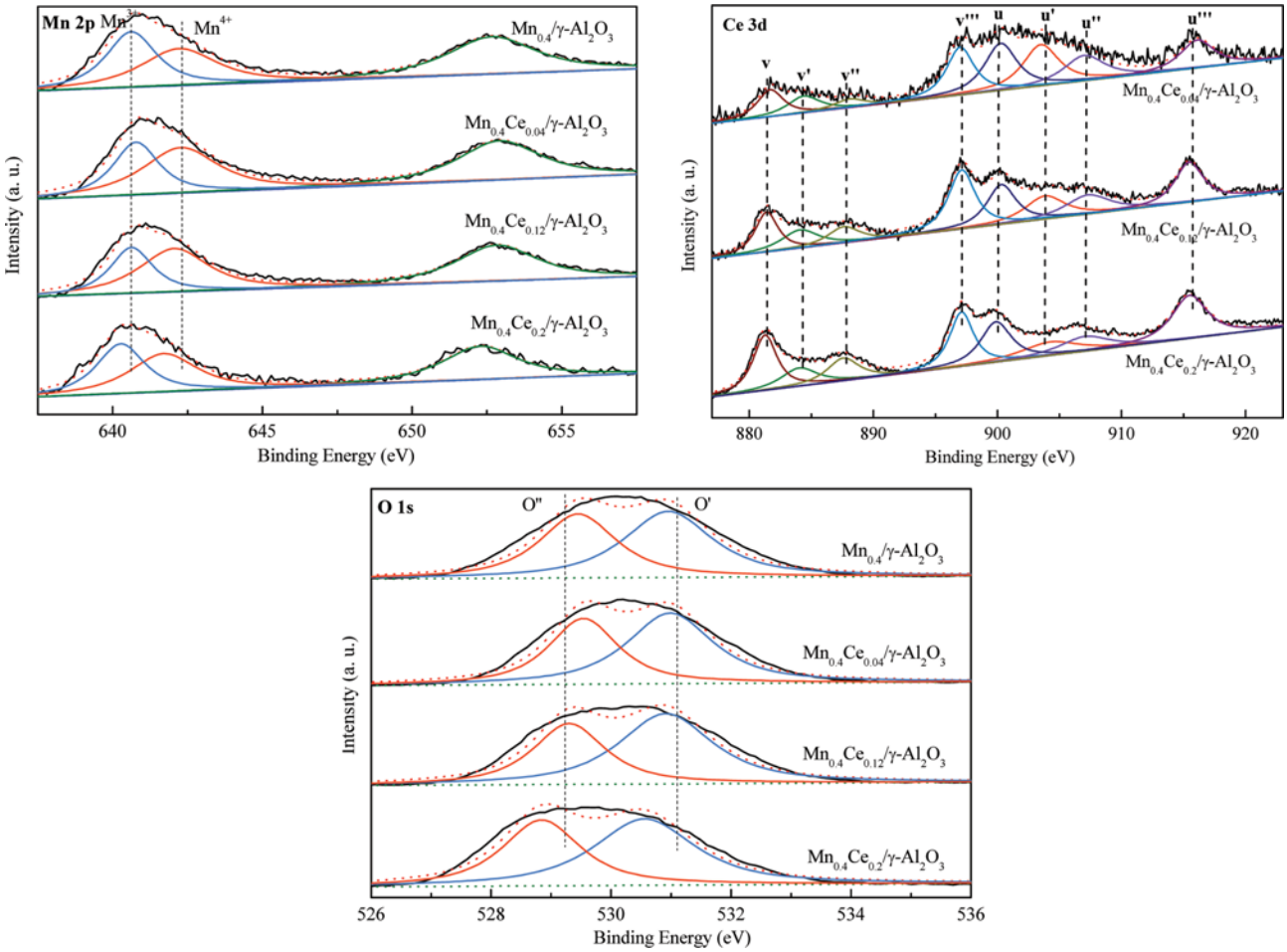

Fig. 4. XPS spectras of O 1s, Ce 3d and Mn 2p for different catalysts.

nia sulfate to cover the catalyst surface. Combining the characterization results and catalytic activity, it can be concluded that Ce modified catalyst, especially for $Mn_{0.4}Ce_{0.12}/\gamma$-Al_2O_3, has a larger surface areas and higher active component dispersion degree, which makes more active sites exposed on the catalyst surface. For $Mn_{0.4}Ce_{0.12}/\gamma$-Al_2O_3, when the formed ammonia sulfate covers the catalyst surface the active sites remained can still play roles in SCR activity. Furthermore, XPS results show that $Mn_{0.4}Ce_{0.12}/\gamma$-Al_2O_3 has more surface adsorbed oxygen and Mn^{4+} which plays a more important role in SCR activity. Therefore, $Mn_{0.4}Ce_{0.12}/\gamma$-Al_2O_3 has a better SO_2 resistance.

2-3. Optimized Structures and Models

As shown in XRD results, MnO_2 and CeO_2 were main crystalline states on the catalyst surface. And XPS results showed that atomic concentrations of Mn^{4+} and Ce^{4+} were a little higher than that of Mn^{3+} and Ce^{3+}. Furthermore, previous studies have pointed

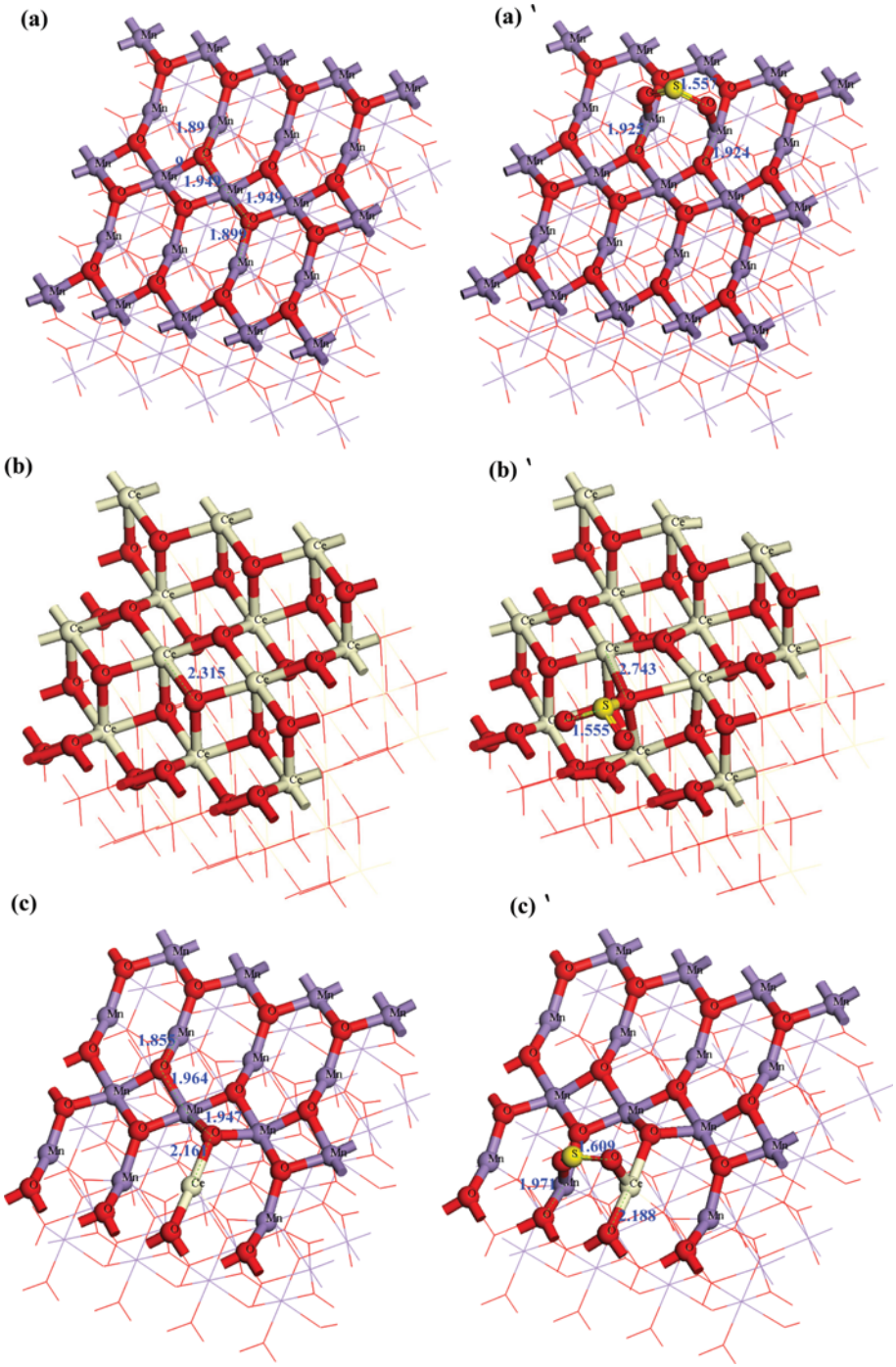

Fig. 5. The optimized structure of (a) MnO_2 (110), (b) CeO_2 (110), (c) Ce doped Mn (110) surfaces and (a)′, (b)′, (c)′ corresponding surfaces adsorbed SO_2. The red balls are oxygen, purple balls are manganese, gray balls are cerium, yellow ball is sulfur.

out that CeO_2 (1 1 0) [35] and MnO_2 (1 1 0) [36] play an important role during the catalytic reaction. Therefore, the MnO_2 (110) and CeO_2 (110) models were built. The effects of Ce doping on the adsorption of SO_2 on MnO_2, CeO_2, MnCe (1 1 0) surface were optimized. SO_2 adsorption energy on different sites was calculated. The optimized structure of MnO_2 (110), CeO_2 (110), Ce doped Mn (110) surfaces and the SO_2 adsorption structures with highest SO_2 adsorption energy are shown in Fig. 5. The other SO_2 adsorption structures are shown in Fig. S1. The Mn-O and Ce-O bond length was 1.949 and 2.315 Å for MnO_2 (1 1 0) and CeO_2 (1 1 0) surface, respectively. These results agree with the other GGA studies [37,38]. After Ce doping, Mn-O bond with length of 1.949 Å was replaced by Ce-O with length of 2.161 Å and Mn-O band length in the position without Ce doping changed from 1.949 to 1.964 and 1.947 Å. It suggested that Ce doping changed MnO_2 (1 1 0) structure considerably at the local position, but it did not change MnO_2 (1 1 0) structure much at the other position. S-O bond length for SO_2 was 1.482 Å, and it increased after being adsorbed on the catalyst surface, and the Ce-O and Mn-O bonds were also changed. These results are due to the interaction between SO_2 and the catalyst surface. The adsorption energy of SO_2 adsorbed on MnO_2, CeO_2, MnCe (1 1 0) was −0.88, −1.21, −1.28 eV, which implied that SO_2 was preferably adsorbed on the Ce surrounding after Ce doping MnO_2 (1 1 0). Thus, Ce doping could protect the main active component MnO_2 from SO_2 poisoning, resulting in a better SO_2 resistance. Ji et al. [39,40] studied the effect of ceria on the sulfation of the catalyst with DRIFTS, and pointed out that ceria was able to store sulfur during catalyst exposure to SO_2. In the present work, DFT calculated results are in good agreement with these experimental results.

2-4. FT-IR Analysis

FT-IR analyses were performed to investigate surface species on the catalysts after 6 h treatment with H_2O and SO_2. As shown in Fig. 6, a strong peak at 1,640 cm^{-1} ascribed to symmetric bending vibration of ammonia cation NH_4^+ was detected in both catalysts, which might be due to the formation of NH_4NO_3 during the SCR reaction [41,42]. Two peaks at 1,047 and 1,390 cm^{-1} were detected in $Mn_{0.4}/\gamma$-Al_2O_3, which might be related to SO_4^{2-} and NH^{4+} showing the existence of $(NH_4)_2SO_4$ or NH_4HSO_4 [43]. But for $Mn_{0.4}Ce_{0.12}/\gamma$-Al_2O_3, the peak at 1,390 cm^{-1} was much weaker and the peak at 1,047 cm^{-1} disappeared. Those results indicate that sulfate species could not easily accumulate on the surface of $Mn_{0.4}Ce_{0.12}/\gamma$-Al_2O_3 during treatment with H_2O and SO_2. Previous studies reported that SO_2 could react with ammonia to form ammonium sulfate which was deposited on the active sites and blocked the active channels of catalyst [13-15]. Therefore, lower formation of ammonium sulfate on the surface of $Mn_{0.4}Ce_{0.12}/\gamma$-Al_2O_3 resulted in a better resistance to H_2O and SO_2.

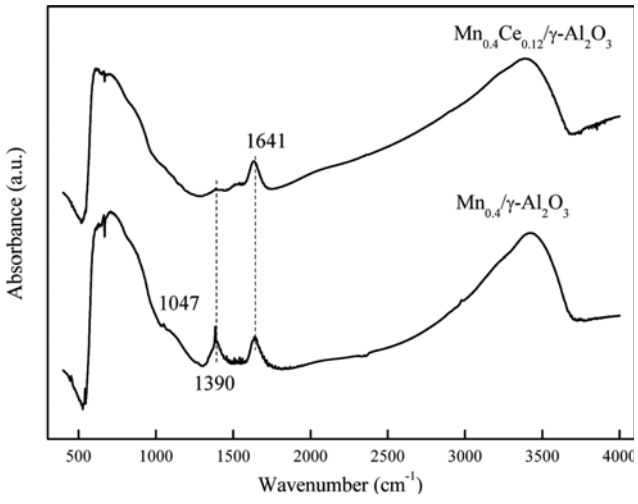

Fig. 6. FT-IR spectrum of the catalysts after 6 h treatment with H_2O and SO_2.

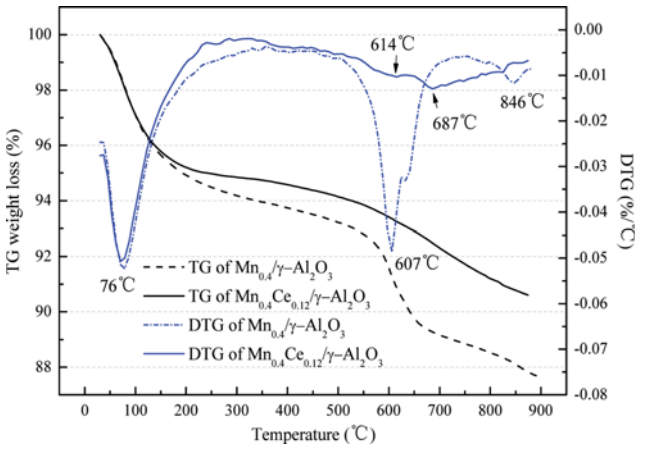

Fig. 7. TG analyses for the catalysts after 6 h treatment with H_2O and SO_2.

2-5. TG Analysis

TG analysis was used to investigate the species and stability of the sulfates on the catalysts surface. As shown in Fig. 7, the sharp peak in DTG trace at 76 °C in both the two catalysts was attributed to the departure of water molecules and hydration. And no visible weight loss stage at 250-350 °C corresponding to decomposition of $(NH_4)_2SO_4$ and NH_4HSO_4 [44] could be found, which indicated that ammonium sulfate could not easily form on the surface of these two catalysts. In $Mn_{0.4}/\gamma$-Al_2O_3, there were two other obvious peaks at 607 and 846 °C which could be assigned to the decomposition of $Al_2(SO_4)_3$ [45] and $MnSO_4$ [11,13]. But for $Mn_{0.4}Ce_{0.12}/\gamma$-Al_2O_3, the peak around 607 °C weakens remarkably and a new weak peak around 687 °C due to $Ce_2(SO_4)_2$ decomposition was observed [11, 46]. Furthermore, no visible peak due to sulfated MnO_x decomposition could be detected in $Mn_{0.4}Ce_{0.12}/\gamma$-Al_2O_3. These results indicate that Ce modification can inhibit sulfate formation on the surface of catalysts, which is in good agreement with the DFT results. Based on the above, Ce modification can change the adsorption energy of SO_2 adsorbed on catalyst surface, lead to the preferential adsorption of SO_2 on Ce surrounding, and inhibit sulfate formation on active component. It has been reported that the formation of sulfates, such as ammonia sulfates and metal sulfates, is the main reason for catalyst deactivation in the presence of SO_2 [47,48]. Ce inhibits sulfates formation on catalyst surface especially on active component MnO_x, which can improve the SO_2 resistance of catalysts, resulting in a better SCR activity in the presence of SO_2.

3. Conclusions

An experimental and DFT study was made to investigate the effects of Ce doped $Mn_{0.4}/\gamma$-Al_2O_3 on SO_2 resistance. DFT results show that Ce modification can change the adsorption energy of SO_2 adsorbed on catalyst surface, resulting in the preferential adsorption of SO_2 on Ce surrounding. FT-IR and TG results show that fewer sulfates can form on the catalyst surface. Therefore, Ce modification inhibiting sulfate formation on active components leads to a high NO conversion in the presence of SO_2.

ACKNOWLEDGEMENTS

This work was supported by the National Natural Science Foundation of China (Grant No. 51408098), the Program for Changjiang Scholars, the Fundamental Research Funds for the Central Universities (Grant No. DUT16RC(4)81) and the State Key Laboratory of fine chemicals (Panjin) project (Grant No. JH2014009).

SUPPORTING INFORMATION

Additional information as noted in the text. This information is available via the Internet at http://www.springer.com/chemistry/journal/11814.

REFERENCES

1. T. Boningari, P. R. Ettireddy, A. Somogyvari, Y. Liu, A. Vorontsov, C. A. McDonald and P. G. Smirniotis, *J. Catal.*, **325**, 145 (2015).
2. S. M. Lee, K. H. Park and S. C. Hong, *Chem. Eng. J.*, **195-196**, 323 (2012).
3. Q. Guo, W. Jing, S. Cheng, Z. Huang, D. Sun, Y. Hou and X. Han, *Korean J. Chem. Eng.*, **32**, 2257 (2015).
4. B. Shen, H. Ma and Y. Yao, *J. Environ. Sci.-China*, **24**, 499 (2012).
5. S. M. Saqer, D. I. Kondarides and X. E. Verykios, *Appl. Catal. B Environ.*, **103**, 275 (2011).
6. F. Cao, J. Xiang, S. Su, P. Wang, S. Hu and L. Sun, *Fuel Process. Technol.*, **135**, 66 (2015).
7. L. Qu, C. Li, G. Zeng, M. Zhang, M. Fu, J. Ma, F. Zhan and D. Luo, *Chem. Eng. J.*, **242**, 76 (2014).
8. M. Wang, H. Liu, Z.-H. Huang and F. Kang, *Chem. Eng. J.*, **256**, 101 (2014).
9. B. Shen, Y. Wang, F. Wang and T. Liu, *Chem. Eng. J.*, **236**, 171 (2014).
10. J. Yu, Z. Si, L. Chen, X. Wu and D. Weng, *Appl. Catal. B Environ.*, **163**, 223 (2015).
11. H. Chang, X. Chen, J. Li, L. Ma, C. Wang, C. Liu, J. W. Schwank and J. Hao, *Environ. Sci. Technol.*, **47**, 5294 (2013).
12. G. S. Qi and R. T. Yang, *J. Catal.*, **217**, 434 (2003).
13. J. Yu, F. Guo, Y. L. Wang, J. H. Zhu, Y. Y. Liu, F. B. Su, S. Q. Gao and G. G. Xu, *Appl. Catal. B Environ.*, **95**, 160 (2010).
14. F. D. Liu and H. He, *Catal. Today*, **153**, 70 (2010).
15. F. Cao, S. Su, J. Xiang, P. Wang, S. Hu, L. Sun and A. Zhang, *Fuel*, **139**, 232 (2015).
16. B. X. Shen, X. P. Zhang, H. Q. Ma, Y. Yao and T. Liu, *J. Environ. Sci.-China*, **25**, 791 (2013).
17. Q. Zhang, Z. Song, P. Ning, X. Liu, H. Li and J. Gu, *Catal. Commun.*, **59**, 170 (2015).
18. Z. Wu, R. Jin, H. Wang and Y. Liu, *Catal. Commun.*, **10**, 935 (2009).
19. R. Jin, Y. Liu, Y. Wang, W. Cen, Z. Wu, H. Wang and X. Weng, *Appl. Catal. B Environ.*, **148**, 582 (2014).
20. P. Yang, X. M. Xue, Z. H. Meng and R. X. Zhou, *Chem. Eng. J.*, **234**, 203 (2013).
21. B. Delley, *J. Chem. Phys.*, **92**, 508 (1990).
22. B. Delley, *J. Chem. Phys.*, **113**, 7756 (2000).
23. J. P. Perdew, K. Burke and M. Ernzerhof, *Phys. Rev. Lett.*, **77**, 3865 (1996).
24. G. Qi and R. T. Yang, *J. Phys. Chem. B*, **108**, 15738 (2004).
24. W. H. Baur, *Acta Crystallogr B*, **32**, 2200 (1976).
25. O. T. Sørensen, *J. Solid State Chem.*, **18**, 217 (1976).
26. A. Laachir, V. Perrichon, A. Badri, J. Lamotte, E. Catherine, J. C. Lavalley, J. El Fallah, L. Hilaire, F. Le Normand and E. Quéméré, *J. Chem. Soc., Faraday Trans.*, **87**, 1601 (1991).
27. D. H. Shang, W. Cai, W. Zhao, Y. F. Bu and Q. Zhong, *Catal. Lett.*, **144**, 538 (2014).
28. B. Thirupathi and P. G. Smirniotis, *Appl. Catal. B Environ.*, **110**, 195 (2011).
29. A. Sultana, M. Sasaki and H. Hamada, *Catal. Today*, **185**, 284 (2012).
30. J. L. Xie, D. Fang, F. He, J. F. Chen, Z. B. Fu and X. L. Chen, *Catal. Commun.*, **28**, 77 (2012).
31. G. Qi and R. T. Yang, *J. Phys. Chem. B*, **108**, 15738 (2004).
32. D. I. Kondarides and X. E. Verykios, *J. Catal.*, **174**, 52 (1998).
33. S. Yang, W. Zhu, Z. Jiang, Z. Chen and J. Wang, *Appl. Surf. Sci.*, **252**, 8499 (2006).
34. Y. Shao, J. Li, H. Chang, Y. Peng and Y. Deng, *Catal. Sci. Technol.*, **5**, 3536 (2015).
35. K. B. Zhou, X. Wang, X. M. Sun, Q. Peng and Y. D. Li, *J. Catal.*, **229**, 206 (2005).
36. D. A. Tompsett, S. C. Parker and M. S. Islam, *J. Am. Chem. Soc.*, **136**, 1418 (2014).
37. G. A. E. Oxford and A. M. Chaka, *J. Phys. Chem. C*, **115**, 16992 (2011).
38. Y. Peng, W. W. Yu, W. K. Su, X. Huang and J. H. Li, *Catal. Today*, **242**, Part B, 300 (2015).
39. Y. Y. Ji, T. Toops and M. Crocker, *Catal. Lett.*, **127**, 55 (2009).
40. Y. Y. Ji, T. J. Toops, J. A. Pihl and M. Crocker, *Appl. Catal. B Environ.*, **91**, 329 (2009).
41. Y. Zhang, X. Zhao, H. Xu, K. Shen, C. Zhou, B. Jin and K. Sun, *J. Colloid Interface Sci.*, **361**, 212 (2011).
42. W. J. Ji, Y. Chen, S. K. Shen, S. B. Li and H. L. Wang, *Appl. Surf. Sci.*, **99**, 151 (1996).
43. H. B. Fu, X. Wang, H. B. Wu, Y. Yin and J. M. Chen, *J. Phys. Chem. C*, **111**, 6077 (2007).
44. L. Mao, T. Ali, C. Huang and N. Z. Muradov, *Int. J. Hydrogen Energy*, **36**, 5822 (2011).
45. W. S. Kijlstra, M. Biervliet, E. K. Poels and A. Bliek, *Appl. Catal. B Environ.*, **16**, 327 (1998).
46. W. Xu, H. He and Y. Yu, *J. Phys. Chem. C*, **113**, 4426 (2009).
47. M. Casapu, O. Kröcher and M. Elsener, *Appl. Catal. B Environ.*, **88**, 413 (2009).
48. Z. P. Zhu, Z. Y. Liu, S. J. Liu, H. X. Niu, T. D. Hu, T. Liu and Y. N. Xie, *Appl. Catal. B Environ.*, **26**, 25 (2000).

Supporting Information

Mechanism of Ce promoting SO_2 resistance of MnO_x/γ-Al_2O_3: An experimental and DFT study

Xiaopeng Zhang*, Zhuofeng Li*, Jijun Zhao, Yuezong Cui*, Bojian Tan*, Jinxin Wang*, Chengxiang Zhang*, and Gaohong He*,†**

*School of Petroleum and Chemical Engineering, State Key Laboratory of Fine Chemicals, Dalian University of Technology, Panjin 124221, Liaoning, China
**Key Laboratory of Materials Modification by Laser, Ion and Electron Beams (Dalian University of Technology), Ministry of Education, Dalian 116024, China
(*Received 6 July 2016 • accepted 1 April 2017*)

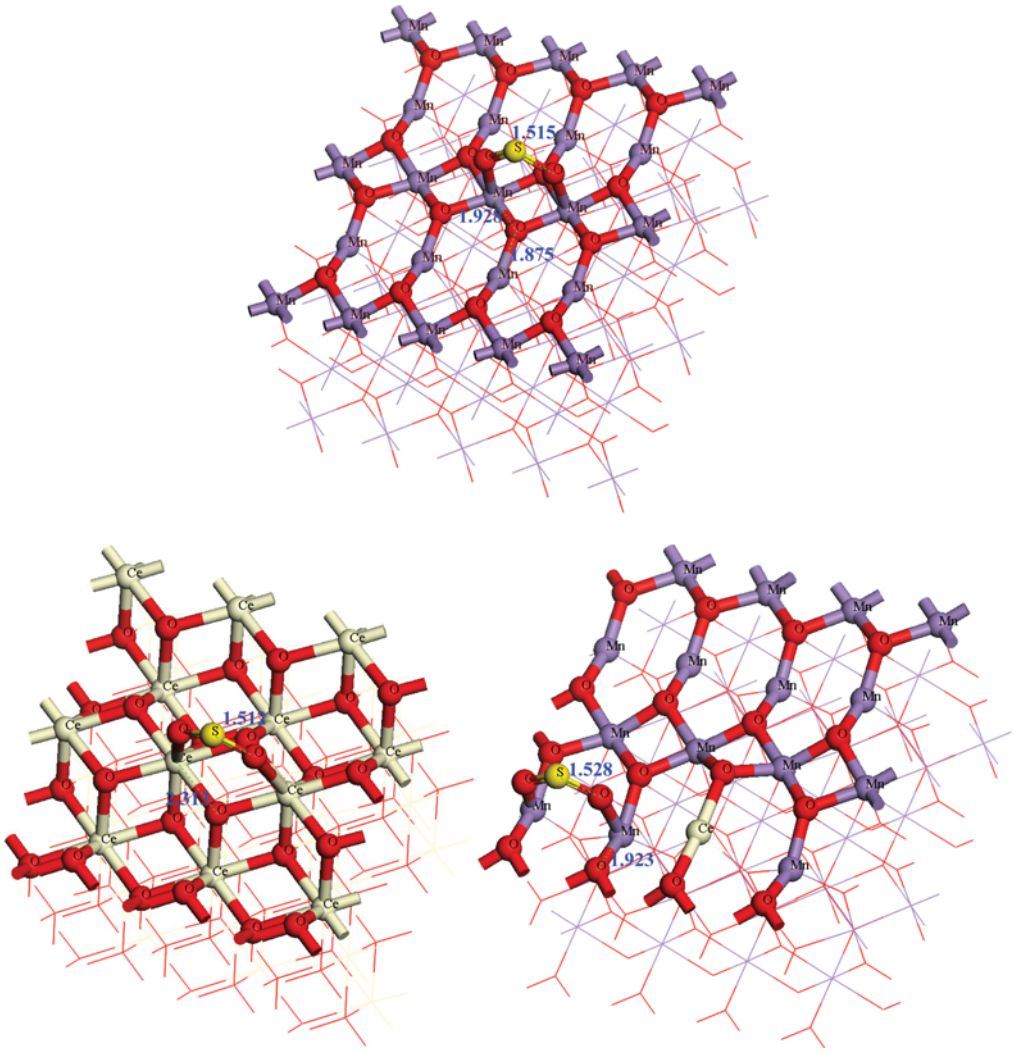

Fig. S1. The optimized structure of SO_2 adsorbed on (a) MnO_2 (110), (b) CeO_2 (110), (c) Ce doped Mn (110) surfaces. The red balls are oxygen, purple balls are manganese, gray balls are cerium, yellow ball is sulfur.

The adsorption energy of SO_2 adsorbed on MnO_2, CeO_2, MnCe (1 1 0) were −0.31, −0.50, −0.67 eV.